Journal of Materials Chemistry A

Accepted Manuscript

This is an *Accepted Manuscript*, which has been through the Royal Society of Chemistry peer review process and has been accepted for publication.

Accepted Manuscripts are published online shortly after acceptance, before technical editing, formatting and proof reading. Using this free service, authors can make their results available to the community, in citable form, before we publish the edited article. We will replace this *Accepted Manuscript* with the edited and formatted *Advance Article* as soon as it is available.

You can find more information about *Accepted Manuscripts* in the Information for Authors.

Please note that technical editing may introduce minor changes to the text and/or graphics, which may alter content. The journal's standard Terms & Conditions and the Ethical guidelines still apply. In no event shall the Royal Society of Chemistry be held responsible for any errors or omissions in this *Accepted Manuscript* or any consequences arising from the use of any information it contains.

ROYAL SOCIETY OF CHEMISTRY

www.rsc.org/materialsA

Understanding the Mechanism of Hydrogenated $NiCo_2O_4$ Nanograss Supported on Ni Foam for Enhanced-Performance Supercapacitors

D. S. Sun, Y. H. Li, Z. Y. Wang, X. P. Cheng, S. Jaffer, Y. F. Zhang*

Institute of Microstructure and Property of Advanced Materials, Beijing University of Technology, Beijing 100124, P. R. China

D. S. Sun and Y. H. Li are both contributed equally.

*Corresponding authors: (Y. Z. yfzhang@bjut.edu.cn)

Spinel $NiCo_2O_4$ is considered a promising supercapacitive material because of its high theoretical capacity (greater than 3000 F g^{-1}), nontoxicity, and safety. Here, we report that electrodes of porous $NiCo_2O_4$ nanograss grown *in situ* and supported on Ni foam achieved remarkable enhancement in electrochemical performance through facile hydrogenation at 300°C for time periods of 1-4 h. The electrodes synthesized via 3 h of hydrogenation (H-$NiCo_2O_4$-3 h) exhibited superior comprehensive electrochemical performance compared with the pristine pattern (air-annealed). The peak value of the area capacitance improved from the pristine 0.88 F cm^{-2} (338.5 F g^{-1}) to 2.1 F cm^{-2} (807.7 F g^{-1}) of H-3 h, an increase of ~240 %. Additionally, the capacity retention from 1 to 30 mA cm^{-2} improved to a value of 71 % (H-$NiCo_2O_4$-3 h), which was superior to that of non-hydrogenated samples (54 %). Furthermore, the long-cycling performance at 10 mA cm^{-2} exhibited a capacitance activation H-$NiCo_2O_4$-3h within the first 1000 cycles, from 2.4 (923 F g^{-1}) to 3.2 F cm^{-2} (1230 F

Journal of Materials Chemistry A Accepted Manuscript

g^{-1}), and declined to 1.5 F cm^{-2} (577 F g^{-1}) after another 2000 cycles; the last value is still greater than that of the pristine pattern (1.3 F cm^{-2} (500 F g^{-1})). The prominent electrochemical capacitive properties of hydrogenated $NiCo_2O_4$ are attributed to enhancement in the electrical conductivity observed by *in situ* TEM electrical test, resulting from the formation of oxygen vacancies in disordered surface layers (~ 5 nm) observed in the hydrogenated samples based on *in situ* transmission electron microscopy characterization. Our findings provide a scientific explanation for the remarkable hydrogenation-induced electrochemical performance of cobalt oxide or binary nickel cobaltite compounds and offer a new route for the large-scale production of high-performance supercapacitor electrodes.

Introduction

Renewable and clean power sources and energy storage[1-3] have been long-sought objectives, with many efforts devoted toward developing high-performance batteries[4, 5] and supercapacitors (SCs).[6] In recent years, SCs have attracted considerable interest as energy-storage devices because of their advantages of outstanding power density, a fast charge-discharge process and a long cycle life.[7,8] Therefore, many materials have been considered for use as SC electrodes, including carbon-based materials based on forming two charge layer on the contact surface of the electrode material and the electrolyte,[8-11] conducting polymers derived from the rapid and reversible redox reaction of N-type or P-type doped and de-doped in the polymer conjugated chain [12,13] and both noble and transition metal oxides through redox reactions occurred in the

Journal of Materials Chemistry A Accepted Manuscript

interface of electrode material and electrolyte.[14,15] Among the candidate electrode materials, transition metal oxides with highest theoretically specific capacity and low cost, such as NiO,[16-18] V_2O_5,[19]and MnO_2,[20] have received especially strong interest. In particular, spinel cobalt oxides (Co_3O_4) and binary nickel cobaltite compounds ($NiCo_2O_4$) exhibit many exceptional characteristics, such as good redox activity, high capability, and extremely high theoretical specific capacitance, thus suggesting that they are the most promising electrode materials for next-generation SCs.[21-25]

Over the past few years, much research has been focused on developing new strategies to improve the electrochemical properties of $NiCo_2O_4$ nanomaterials for SC electrodes. Notable progress, such as exploring the core-shell structures of compounds like $NiCo_2O_4$@MnO_2[26], $NiCo_2O_4$@$NiCo_2O_4$[27], Co_3O_4@$NiCo_2O_4$,[28] NSs@HMRAs,[29] growing $NiCo_2O_4$ nanosheets on flexible carbon fabric to improve conduction[30] and yolk-shell Ni-Co mixed oxide nanoprisms,[31] has been made. All of this work greatly increased the electrochemical performance of $NiCo_2O_4$ for SC electrodes. However, most of these compounds have limitations, such as high cost triggered by the complex process or being difficult to utilize in industrial applications. Hydrogenation, regarded as the green and effective way to modify the structure, has been applied in improving the performance of TiO_2[32], MnO_2[33], MoO_3[34] and $NiCo_2O_4$ double-shell hollow sphere.[35] While few research has been focused on the properties and mechanism of hydrogenated $NiCo_2O_4$ nanograss. In this context, we have a pressing need for a fundamental understanding of the correlation between the capacitive enhancement and microstructure of $NiCo_2O_4$ electrodes.

Journal of Materials Chemistry A Accepted Manuscript

In this paper, we report a simple and cost-effective approach that employs hydrogenation to improve the performance of $NiCo_2O_4$ nanograss on Ni foam for SC electrode applications. After hydrogenation, the synthesized electrode exhibited large increases in capacitive performance (from 0.88 F cm^{-2} (338.5 F g^{-1}) in the initial state to 2.1 F cm^{-2} (807.7 F g^{-1}) after 3 h of hydrogenation). Moreover, the capacity retention was remarkably promoted from 54 to 71 % at high current density after 3 h of hydrogenation. We attribute this significantly improved electrochemical performance to enhanced electrical conductivity observed by *in situ* TEM electrical test, resulting from oxygen vacancies forming in the disordered structure on the surface of the hydrogenated $NiCo_2O_4$ (H-$NiCo_2O_4$) nanowires (NWs). Our work not only proposes a simple route for improving the capacitance of $NiCo_2O_4$ but also provides a guideline for developing green and performance-enhanced supercapacitors.

Experimental section

Material synthesis

Porous $NiCo_2O_4$ nanograss was fabricated on Ni foam via a one-step hydrothermal method combined with a post-thermal treatment. Cobalt nitrate, ammonium fluoride, and urea were obtained from Beijing Chemical Reagent Company. In a typical synthesis, 0.58 g of $Co(NO_3)_2 \cdot 6H_2O$, 0.18 g of NH_4F, and 1.2 g of $Co(NH_2)_2$ were dissolved in distilled water (35 mL) to form a pink homogeneous solution. The solution was transferred into Teflon-lined stainless steel autoclave liners (50 mL). Then, a piece of clean Ni foam (2 cm x 1 cm) was immersed into the reaction solution. The top of the foam (1 cm x 1 cm) was protected from solution contamination by

Journal of Materials Chemistry A Accepted Manuscript

uniformly coating the top with polytetrafluoroethylene tape. The liner was sealed in a stainless steel autoclave and then held at 120 °C for 6 h. The Ni foam coated with black precursor was collected and rinsed with distilled water and ethanol several times before drying at 70 °C for 3 h. Finally, the precursor was annealed at 300 °C in ambient atmosphere for 2 h, thus producing porous $NiCo_2O_4$ nanograss.

The H-$NiCo_2O_4$ was prepared by keeping porous $NiCo_2O_4$ in a hydrogen environment at 300 °C for 1, 2, 3 or 4 h (denoted H-$NiCo_2O_4$-1 h, H-$NiCo_2O_4$-2 h, H-$NiCo_2O_4$-3 h, and H-$NiCo_2O_4$-4 h, respectively).

To calculate the mass loading on the Ni foam accurately, the ICP atomic emission spectrometer (ICP-AES) was applied in the experiment (shown in supporting information, table S1). Through the calculation, we got that the mass loading of $NiCo_2O_4$ was 2.6 mg.

Structural characterization

The crystal structure of as-synthesized samples was characterized via X-ray diffraction (XRD; Bruker, D8 Discover) with Cu Kα radiation (λ = 0.154 nm). The morphology and structure were obtained via scanning electron microscopy (SEM; FEI, Quanta 650), transmission electron microscopy (TEM; JOEL, JEM-2010), and high-resolution TEM (HRTEM; JOEL, JEM-2010 F). *In situ* electrical measurement experiments were performed using a commercial scanning tunneling microscope-TEM (STM–TEM; Nanofactory Instruments) joint instrument insert into a JOEL-2010 TEM. The valence state and oxygen vacancies were characterized via electron energy loss spectroscopy (EELS; JOEL, JEM-2010F) and X-ray

Journal of Materials Chemistry A Accepted Manuscript

photoelectron spectroscopy (XPS; PHI Quantera SXM with Al Kα radiation). The EDS was carried out on transmission electron microscopy (TEM; FEI-T20).

Electrochemical tests

A typical three-electrode cell (including a working electrode, a platinum foil counter electrode, and an Hg/HgO electrode as the reference electrode) was used for measuring the working electrode. The electrochemical measurements were performed under immersion using 6 M KOH as the electrolyte. Cyclic voltammetry (CV) measurements were performed using a CHI660E electrochemical workstation, with the $NiCo_2O_4$ nanograss – Ni foam composite (1 cm^2 area) as the working electrode. The galvanostatic charge-discharge tests were conducted using a LAND battery test system (LAND, Wuhan). Electrochemical impedance spectroscopy (EIS) was performed at open circuit potential with an ac perturbation of 5 mV in the frequency range of 100 kHz to 0.01 Hz.

Journal of Materials Chemistry A Accepted Manuscript

Results and discussion

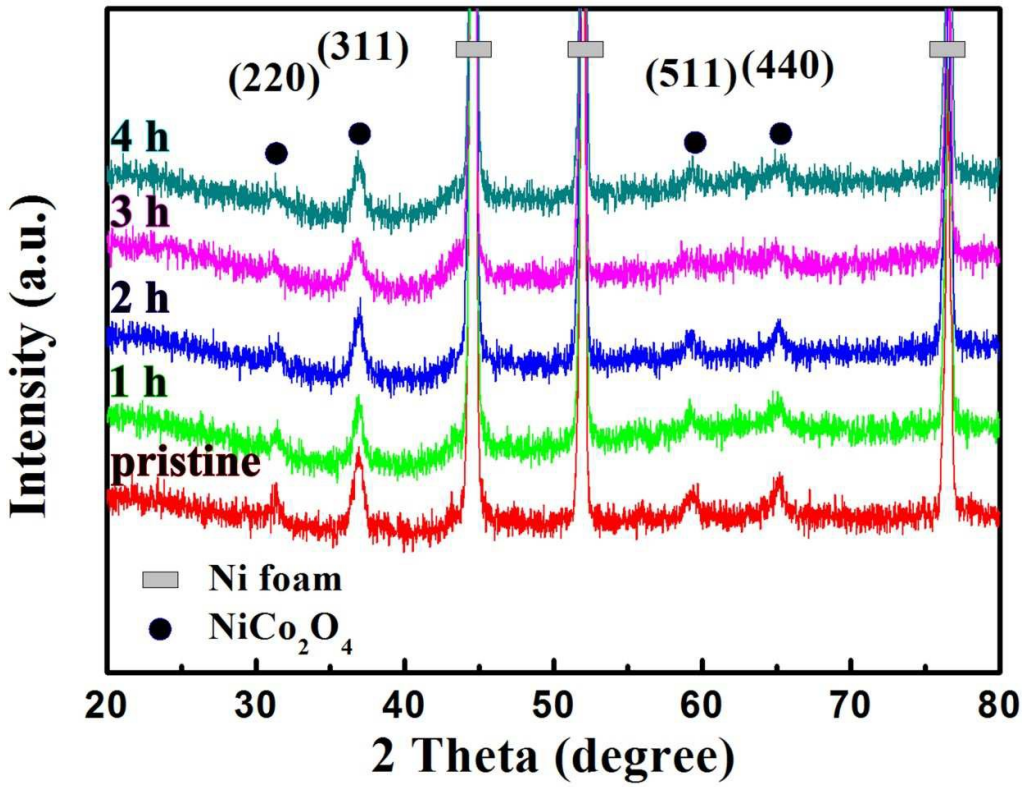

Fig. 1 XRD patterns of pristine $NiCo_2O_4$ and H-$NiCo_2O_4$ samples. From the bottom to the top, the spectra correspond to the pristine, H-$NiCo_2O_4$ 1 h, H-$NiCo_2O_4$ 2 h, H-$NiCo_2O_4$ 3 h, and H-$NiCo_2O_4$ 4 h samples.

Typical XRD spectra of the synthesized samples (pristine and hydrogenated) are presented with different colors in Fig. 1. The diffraction peaks, except for the three typical peaks from the Ni foam, and the atomic ratio of nickel, cobalt and oxide is approximately 1:2:4 evidenced by EDS result shown in Fig. S1a, can be jointly proved to be spinel $NiCo_2O_4$ (JCPDS no. 20-0781). It can be observed that the spectra do not exhibit any obvious differences, demonstrating that the structure of the hydrogenated samples was not notably changed relative to that of the pristine samples.

Journal of Materials Chemistry A Accepted Manuscript

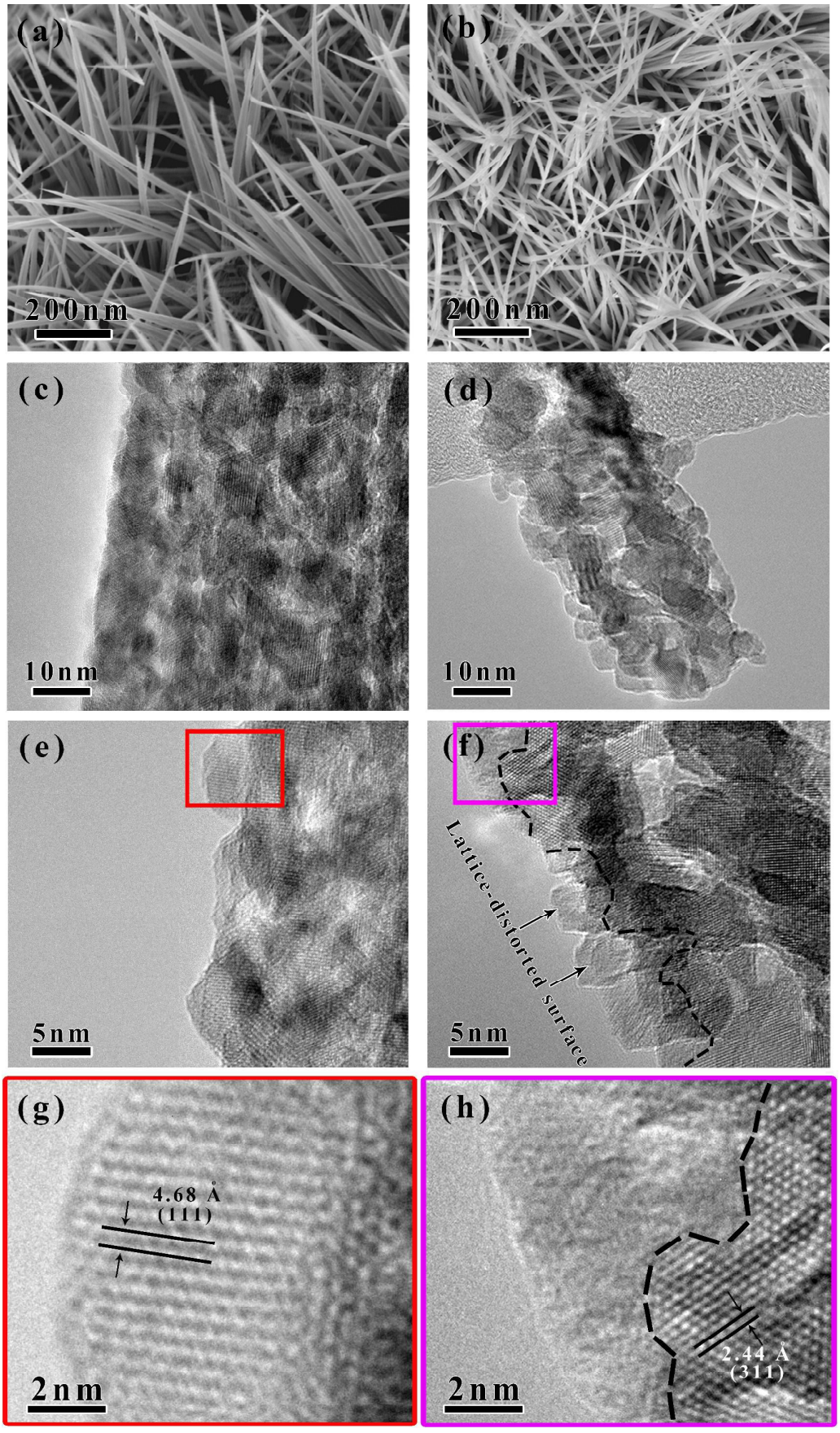

Journal of Materials Chemistry A Accepted Manuscript

Fig. 2 Structural characterization of pristine $NiCo_2O_4$ and H-$NiCo_2O_4$ patterns. (a) SEM image and (c) TEM image, (e, g) HRTEM images of pristine $NiCo_2O_4$; (b) SEM image and (d) TEM image, (f, h) HRTEM images of H-$NiCo_2O_4$.

The deep insight of structural and morphological characteristics of the as-prepared hybrid products can be shown in Fig. 2. According to the TEM image shown in Fig. S1b-f, the nanograss was composed of NWs of which the average diameter and length is about 100-200 nm and 2 μm, respectively. The TEM images and corresponding diffraction patterns indicate the same results that only well-crystalline $NiCo_2O_4$ phase appeared validated by XRD spectrum (Fig. 1). SEM images of the pristine and H-$NiCo_2O_4$-3 h nanograss are presented in Fig. 2a, b; the images indicate that the H-$NiCo_2O_4$-3 h (Fig. 2b) nanograss softened after hydrogenation. Other SEM images of the hydrogenated samples (1 h, 2 h, and 4 h) presented in Fig. S2 show that with extension of treated time in hydrogen, the phenomenon of softened nanograss appeared, especially in H-$NiCo_2O_4$-3 h and H-$NiCo_2O_4$-4 h samples. The gradual magnified HRTEM of pristine $NiCo_2O_4$ and H-$NiCo_2O_4$-3 h nanowires are shown in Fig. 2c,e,g and d,f,h respectively. As can be seen from Fig. 2c,e,g the individual NW is mesporous structure and well crystallized with clearly resolved lattice fringes of $NiCo_2O_4$ (Fig. 2c,e). The adjacent-plane distance of 0.468 nm of pristine pattern corresponds well to the (110) plane of $NiCo_2O_4$ structure (Fig. 2g). H-$NiCo_2O_4$-3 h images shown in Fig 2d, demonstrate the same porous structure, showing non-damage happened compared to pristine one, however, it is worth to mentioning that a uniformly lattice-distorted surface (~ 5 nm) marked by dash line in Fig. 2f emerged in

Journal of Materials Chemistry A Accepted Manuscript

H-$NiCo_2O_4$-3h samples, and its partially enlarged detail exhibited in Fig. 2h, reveal the obviously appeared interface between lattice-distorted surface and crystalline region where 0.244 nm of the adjacent-plane distance is consistent with the (311) plane of $NiCo_2O_4$ crystal.

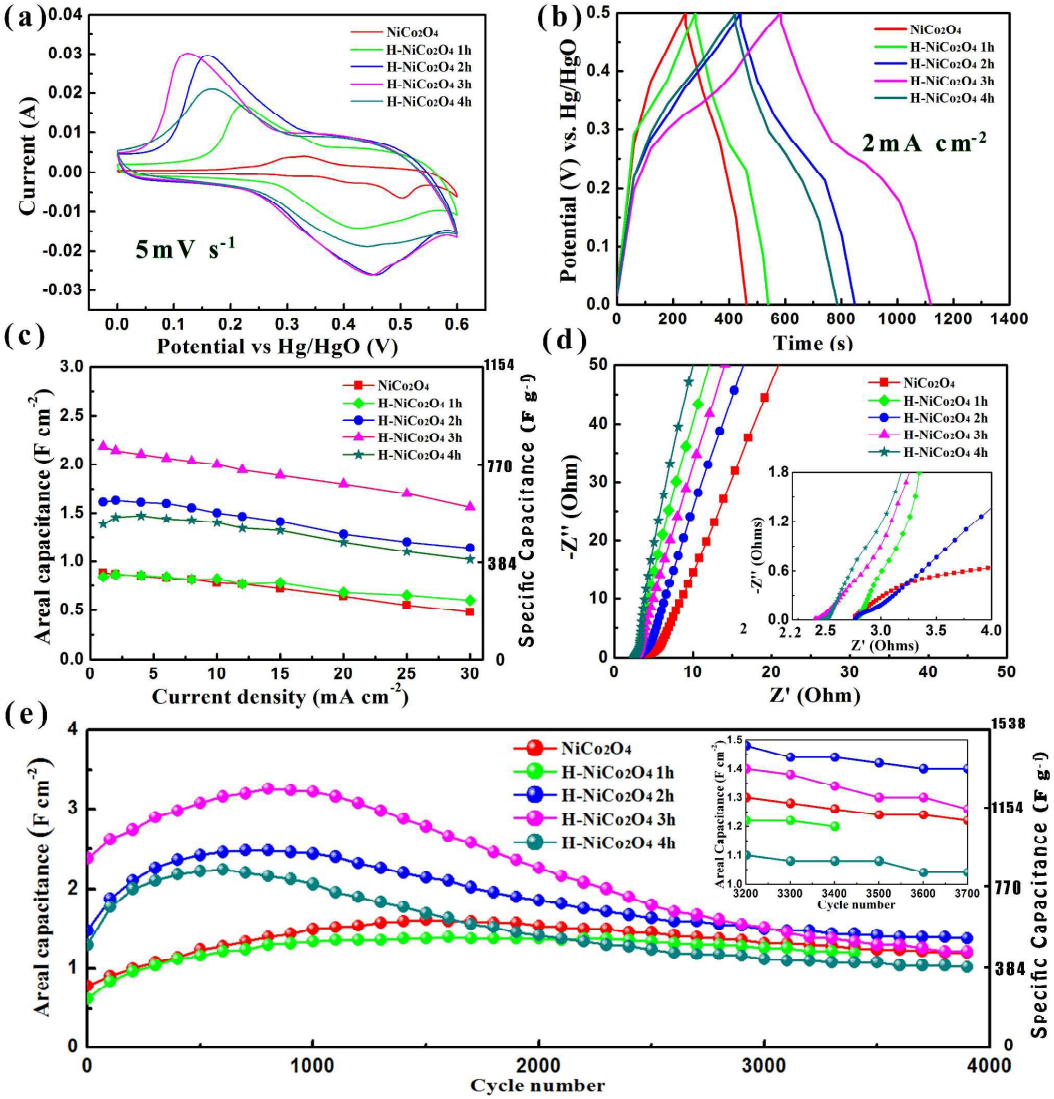

Fig. 3 Electrochemical performance of pristine $NiCo_2O_4$ and different H-$NiCo_2O_4$ samples; t. Comparison of (a) CV curves, (b) galvanostatic charge-discharge curves at 2 mA cm^{-2}, and (c) areal capacitance of pristine $NiCo_2O_4$ samples and H-$NiCo_2O_4$ samples, showing that capacitance enhancement after hydrogenation. (d) Nyquist plots, and (e) cycling performance at a current density of

Journal of Materials Chemistry A Accepted Manuscript

10 mA/cm^2; the H-$NiCo_2O_4$-3 h sample exhibited still 15% increase relative to the pristine sample after 3200 cycles.

Hence, samples prepared in pristine and hydrogenated environments for use as the electrode in supercapacitors were tested and compared. CV tests were performed on Ni foam, the pristine $NiCo_2O_4$-Ni foam nanograss and hydrogenated specimens. On the basis of the CV curves of Ni foam (Fig. S5), the performance of Ni foam has little influence on the electrochemical performance of $NiCo_2O_4$ and even H-$NiCo_2O_4$. And the CV curves of the initial $NiCo_2O_4$ and H-$NiCo_2O_4$ are shown in Fig. 3a at a scanning rate of 5 mV s^{-1}. It is notable that the enclosed separation area increased greatly after hydrogenation, and a peak value emerged in hydrogenating 3h, which indicated that the capacitance of H-$NiCo_2O_4$ samples is much higher than that of pristine one. All of the curves include a pair of broad peaks, which are the characteristic peaks of faradic reaction for M-O/M-O-OH (M = Ni or Co) in KOH electrolyte.

The galvanostatic charge-discharge curves of the as-prepared pristine and H-$NiCo_2O_4$ samples with a potential window of 0-0.5 V were conducted at different charge-discharge current densities ranging from 1 to 10 mA cm^{-2} (Fig. 3b). The discharge time of H-3 h samples got peak at current density of 2 mA cm^{-2}. The variation in the specific capacitance derived from the galvanostatic charge/discharge process as a function of current density of discharge for the pristine and H- $NiCo_2O_4$ is plotted in Fig. 3c. The pristine $NiCo_2O_4$-Ni sample exhibited a capacitance of 0.88 F cm^{-2} (338.5 F g^{-1}) at 1 mA cm^{-2}, whereas the H-$NiCo_2O_4$ samples (at different rates)

Journal of Materials Chemistry A Accepted Manuscript

exhibited varying high capacitance levels, all of which exceed the initial value. The H-$NiCo_2O_4$ 3 h sample exhibited a surprisingly high capacitance of as much as 2.13 F cm^{-2} (819.2 F g^{-1}), which is 240 % greater than the original value. The hydrogenation induced capacity enhancement is much greater than hierarchical complex composites, such as, $NiCo_2O_4$@MnO_2,[26] $NiCo_2O_4$@ppy,[44] and even $NiCo_2O_4$ with conductive additions like $NiCo_2O_4$@RGO,[45] demonstrating the significant advantage of facile hydrogenation in improving the capacitive performance. In addition, the H-$NiCo_2O_4$ samples exhibited better rate capability than the initial $NiCo_2O_4$ samples. The $NiCo_2O_4$ samples that were hydrogenated for 1, 2, 3, and 4 h had 82, 70, 71, and 73 % retention, respectively, at a current density of 30 mA cm^{-2}, whereas the initial samples had only 54 % capacitive retention. The obtained Nyquist plots shown in Fig. 3d consist of a depressed arc in the high-frequency region and a linear component in the low-frequency region. The internal resistance (R_b), which includes the sum of the resistance of the active material, the electrolyte resistance, and the contact resistance of the active material/current collector interface, can be acquired from the intercept of the plots on the real axis. As observed from the inset of Fig. 3d, the R_b of pristine sample and the hydrogenated samples treated for 1, 2, 3, or 4 h were 2.76, 2.78, 2.76, 2.39, and 2.46, respectively, indicating enhancement in the ion diffusion and effective electron transfer in the electrode charge-discharge process. As to the increased R_b of H- 4h sample, this is mainly due to the electrical contact loss between $NiCo_2O_4$ nanograss and Ni foam caused by the long annealing time. It can be observed that more cracks appeared, especially in the H- $NiCo_2O_4$-4 h samples, as shown in Fig.

Journal of Materials Chemistry A Accepted Manuscript

S3e.

The cyclic stability of the pristine and H-$NiCo_2O_4$ nanograss-Ni foams was measured at current density of 10 mA cm^{-2}. As shown in Fig. 3e, the cycling period can be divided into two sections: the active section and the capacity loss section.[42] It is found that the initial $NiCo_2O_4$ samples achieved their peak after 1500 cycles and then exhibited a slow decrease in specific capacitance in the 1500-4000 cycle range. The hydrogenated samples exhibited a capacitance activation within the first 700-1000 cycles; and then shown a capacity decline until they reached 3000 cycles. Despite the capacity loss, the last value (1.22 F cm^{-2} (469.2 F g^{-1}) of H-3 h) is still greater than that of the pristine pattern (1.2 F cm^{-2} (461.5 F g^{-1})). This capacity decline behavior might be caused by the loss of active material during charge-discharge cycles, resulting from lower contact force between $NiCo_2O_4$ nanograss and Ni foam with excessive annealing time.

To further study the postmortem $NiCo_2O_4$ electrode during the cycling, the morphology evolution of electrode after 3000th cycle was characterized by TEM (shown in Fig. S6). TEM images reveal that after 3000th charge-discharge cycle, the $NiCo_2O_4$ nanograss were uniformly covered with a 20-50nm length layer, forming a core-shell structure. The SAED patterns (Fig. S6a'', b'', c'') show that both core and shell structure have same $NiCo_2O_4$ crystal structure. The core–shell nanoforest architecture would significantly improve the surface area with respect to the pristine a pattern, and even provide more sites for redox reaction, result in the activation process happened in the cycling period .[42]

Journal of Materials Chemistry A Accepted Manuscript

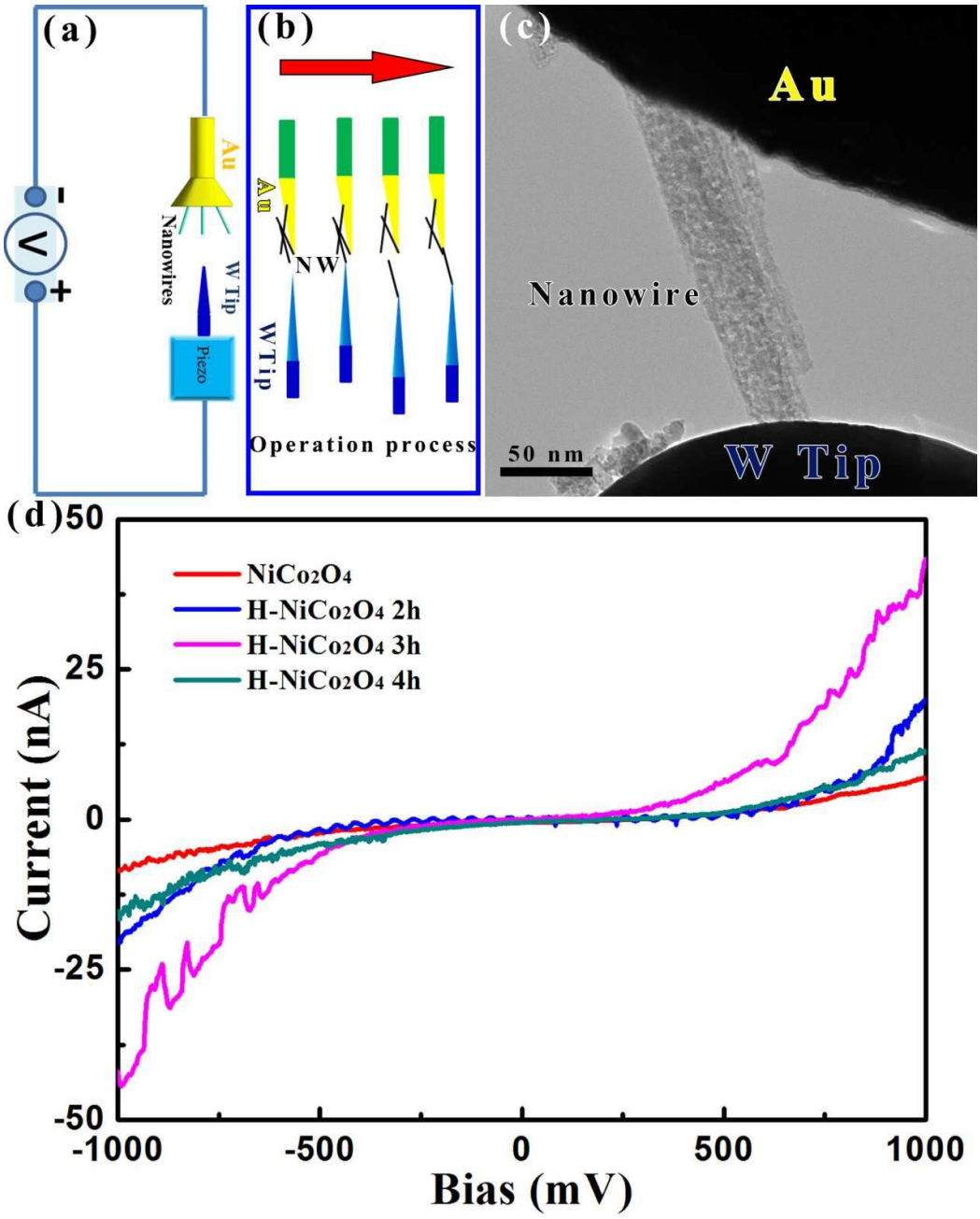

Fig. 4 (a) Schematic representation of *in situ* STM-TEM conductivity test device. (b) Schematic diagram of the specimen operation process. (c) TEM view of an individual $NiCo_2O_4$ NW bridging a W tip and an Au rod. (d) I-V characteristics of single pristine and hydrogenated samples.

I-V curves of the electrical conductivity of the individual pristine and hydrogenated $NiCo_2O_4$ NWs were also obtained using an *in situ* STM-TEM system (Fig. 4a). To

Journal of Materials Chemistry A Accepted Manuscript

ensure the connectivity of the NWs and the Au rod, the W tip is used to pull a NW out, and then inserted the NW onto the surface of a new flat Au rod. A video was recorded shown in Video S1. A schematic diagram of this process is shown in Fig. 4b. The W tip, Au rod and an individual $NiCo_2O_4$ NW were brought into contact to realize a closed loop through the nanoscale precision piezo-driven manipulator of the STM-TEM holder (Fig. 4c). The I-V curves of the pristine and hydrogenated samples were measured and are plotted in Fig. 4d. The current value of the pristine sample varied from 6.8 to -8.5 nA, whereas those of the H-$NiCo_2O_4$-2 h, -3 h and -4 h samples varied from 20.2 to -19.9 nA, from 42 to -43.5 nA and from 15.3 to -11.35 nA, respectively. This result illustrates that drastic enhanced conductivity of the H-$NiCo_2O_4$-3 h pattern happened compared to pristine one and even other hydrogenated times, especially H-$NiCo_2O_4$-4h sample revealing the excess oxygen vacancies may hinder further improvement in the conductivity and electrochemical performance.[41]

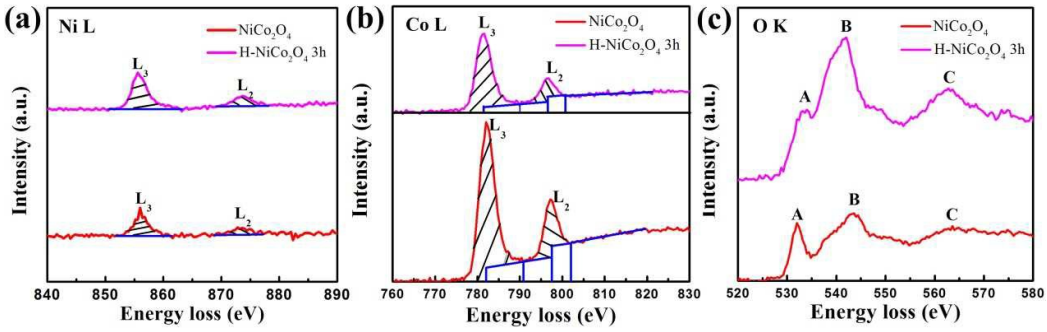

Fig. 5 Valence state characterization of pristine $NiCo_2O_4$ samples and H-$NiCo_2O_4$ 3 h samples. EELS spectra of (a) Ni $L_{2,3}$-edge, (b) Co $L_{2,3}$-edge, and (c) O K-edge.

The structural evolution of the pristine and H-$NiCo_2O_4$-3 h pattern was also studied

Journal of Materials Chemistry A Accepted Manuscript

by *in-situ* electron energy loss spectroscopy (EELS) (Fig. 5). There are many techniques to correlate the EELS signals with the valence states. In this study, we calculated the peak ratios is calculated using a method demonstrated in Fig. 5a, b, [38] integrating the shaded area of peaks to determine the L3/L2 line ratios for Co L-edge[36] and Ni L-edge.[37] The L3/L2 ratios for Co L-edge and Ni L-edge in the initial sample were 1.3 and 3.8, respectively, whereas the corresponding ratios for hydrogenated samples increased to 2.85 and 4.4, respectively. The increased average (Co, Ni) L3/L2 ratio indicates a valence decrease of Co (Co^{3+} to Co^{2+}) after hydrogenation.[38] This finding was confirmed by the change in the oxygen K-edge structure. In the oxygen K-edge spectra shown in Fig. 5c, there are three characteristic peaks, which are labeled as A, B, and C. Peak A, located at 532 eV, is referred to as the O K-edge pre-peak and is attributed to the hybridization of the O 2p-state with the transition metal-3d and is correlated with the unoccupied 3d-band of the transition metal.[39] Peaks B and C originate from hybridized O 2p-transition metal 4 sp bands.[40] The intensity of peak A for hydrogenated samples decreased with respect to peak B, thus indicating the formation of oxygen vacancies.[41] Furthermore, XPS, a technique to study and compare surface oxidation, was also performed to characterize the pristine, H-$NiCo_2O_4$ 3 h and H-$NiCo_2O_4$ 4 h samples (Fig. S4). The formation of oxygen vacancies after hydrogenation was also validated by the XPS results. According to cautiously calculating the XPS result, the increase of oxygen vacancies density can be obviously found with the hydrogenated time extension.

Journal of Materials Chemistry A Accepted Manuscript

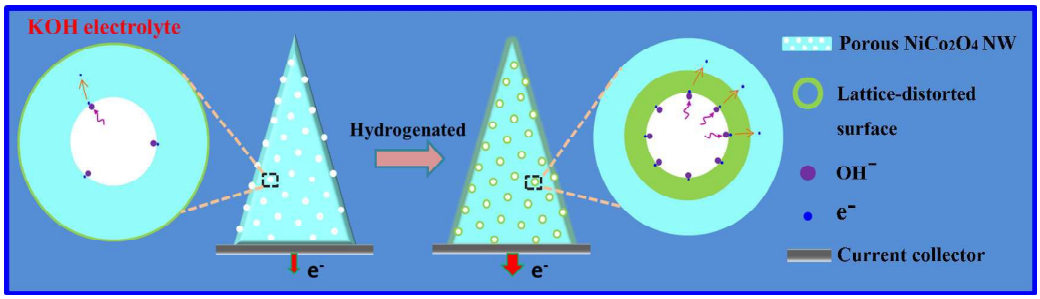

Fig. 6 Schematic diagram illustrating the effect and function of hydrogenation on $NiCo_2O_4$ NWs.

Based on these microstructure investigations, Fig. 6 schematically illustrates the effect and function of hydrogenation on $NiCo_2O_4$ NWs. Because XPS can only probe chemical information within a few atomic layers near the surface, the XPS result indicates that more hydroxyl groups and oxygen vacancies were created in the lattice-distorted region. Surface structural transformations, including oxygen vacancies in lattice-distorted region, enhanced the electrical performance of the NWs to some extent. The redox reaction in the KOH electrolyte are expressed as follows, [27]

$$NiCo_2O_4 + OH^- + H_2O \longleftrightarrow NiOOH + 2CoOOH + e^- \quad (1)$$

$$CoOOH + OH^- \longleftrightarrow CoO_2 + H_2O + e^- \quad (2)$$

Just like the schematic, when the oxidation reaction occurred, electrons would be released. Since the moderate vacancies in lattice-distorted region would greatly facilitate electron transmission, the conductivity of H-$NiCo_2O_4$ samples was significantly increased (Fig. 4d), and thus improved the corresponding electrochemical performance.

Conclusions

In summary, we have demonstrated an enhanced performance electrode with $NiCo_2O_4$ nanograss grown *in situ* on Ni foam using a hydrogenation technique. The

Journal of Materials Chemistry A Accepted Manuscript

electrochemical measurement of H-$NiCo_2O_4$ (duration 3 h) indicated an unexpectedly high specific capacitance (2.1 F cm^{-2} (807.7 F g^{-1})) and excellent rate capability (74 %) values, higher than those exhibited by the pristine sample with the specific capacitance of 0.88 F cm^{-2} (338.5 F g^{-1}) and retention of 54 %, which is ascribed to the moderate formation of oxygen vacancies in lattice-distorted surface of hydrogenated $NiCo_2O_4$ pattern. Therefore, our work not only proposes a simple route for improving the capacitance of $NiCo_2O_4$ but also provides a guideline for developing green and performance-enhanced supercapacitors.

Acknowledgments

This work was supported by the National Natural Science funded project (11374027) and Beijing Natural Science Foundation (2132014).

Notes

D. S. Sun and Y. H. Li are both contributed equally.

References

1 P. Simon, Y. Gogotsi, *Nat. Mater* 2008, **7**, 845-854.

2 T. Chen, L. Qiu, Z. Yang, Z. Cai, J. Ren, H. Li, H. Lin, X, Sun, H. Peng, *Angew. Chem. Int. Ed.*, 2012, **51**, 11977-11980.

3 X. Xiao, L. Yuan, J. Zhong, T. Ding, Y. Liu, Z. Cai, Y. Rong, H. Han, J. Zhou, Z. L. Wang, *Adv. Mater.*, 2011, **23**, 5440-5444.

4 C. K. Chan, H. L. Peng, G. Liu, K. McIlwrath, X. F. Zhang, R. A. Huggins, Y. Cui, *Nature Nanotechnology*, **2008**, 3, 31-35.

5 M. Armand, J.M. Tarascon, *Nature* 2008, **451**, 652-657.

Journal of Materials Chemistry A Accepted Manuscript

6 J.R. Miller, P. Simon, *Science* 2008, **321**, 651-652.

7 D.W. Wang, F. Li, M. Liu, G. Q. Lu and H.M. Cheng, *Angew. Chem, Int. Ed.*, 2008, **120**, 379-382

8 T. Brezesinski, J. Wang, S. H. Tolbert and B. Dunn, *Nat. Mater.*, 2010, **9**, 146-151.

9 L. L. Zhang and X. S. Zhao, *Chem. Soc. Rev.*, 2009, **38,** 2520-2531.

10 E. Raymundo-Pinero, F. Leroux and F. Beguin, *Adv.Mater.*, 2006, **18**, 1877-1882.

11 D. Y. Qu, *J. Power Sources*, 2002, **109,** 403-411.

12 G. A. Snook, P. Kao and A.S. Best, *J. Power Sources*, 2011, **196,** 1-12.

13 E. Frackowiak, V. Khomenko, K. Jurewicz, K. Lota, F. Beguin, *Journal of Power Sources*, 2006, 153, 413-418.

14 W. C. Fang, O. Chyan, C. L. Sun, C. T. Wu, C. P. Chen, K. H. Chen, L. C. Chen and J. H. Huang, *Electrochem. Commun.*, 2007, **9**, 239-244.

15 L. Bao, J. Zang and X. Li, *Nano Lett.*, 2011, **11**, 1215-1220.

16 S. J. Ding, T. Zhu, J. S. Chen, Z. Y. Wang, C. L. Yuan and X. W. Lou, *J. Mater. Chem.*, 2011, **21,** 6602-6606.

17 W. T. Deng, Y. Liu, Y. Zhang, F. Lu, Q. Y. Chen and X. B. Ji, *RSC Adv.*, 2012, **2**, 1743-1745.

18 C. Y. Cao, W. Guo, Z. M. Cui, W. G. Song and W. Cai, *J. Mater. Chem.*, 2011, **21**, 3204-3209

19 B. Saravanakumar, K K. Purushothaman, G. Muralidharan, *ACS Appl. Mater. Interfaces*, 2011, **4**, 4484-4490.

20 Q. T. Qu, P. Zhang, B. Wang, Y. H. Chen, S. Tian, Y. P. Wu and R. Holze, *J. Physical*

Journal of Materials Chemistry A Accepted Manuscript

Chem. C, 2009, **31**, 14020-14027.

21 G. Q. Zhang, H. B. Wu, H. Hoster, M. Chan-Park and X. W. Lou, *Energy Environ. Sci.*, 2012, **5**, 9453-9456.

22 C. Z. Yuan, J. Y. Li, L. R. Hou, X. G. Zhang, L. F. Shen and X. W. Lou, *Adv. Funct. Mater.,* 2012, **22**, 4592-4597.

23 G. Q. Zhang, X. W. Lou, Adv. Mater., 2013, 25, 976-979.

24 Z. Y. Wang, Y. F. Zhang, Y. H. Li and H. Y. Fu, *RSC Adv.*, 2014, **4,** 20234-20238.

25 F. X. Ma, L. Yu, C. Y. Xu and X. W. Lou, *Energy Environ. Sci.*, 2016, DOI: 10.1039/C5EE03772G

26 L. Yu, G. Q. Zhang, C. Z. Yuan and X. W. Lou, *Chem. Commun.*, 2013, **49,** 137-139.

27 X. Y. Liu, S. J. Shi, Q. Q. Xiong, L. Li, Y.J. Zhang, H. Tang, C. D. Gu, X. L. Wang and J. P. Tu, *ACS Appl. Mater. Interfaces*, 2013, **17**, 8790-8795.

28 H. Hu, B. Y. Guan, B. Y. Xia and X. W. Lou, *J. Am. Chem. Soc.,* 2015, **137**, 5590-5595.

29 X. F. Lu, D. J. Wu, R. Z. Li, Q. Li, S. H. Ye, Y. X. Tong and G. R. Li, *J. Mater. Chem. A*, 2014, **2**, 4706-4713.

30 J. Du, G. Zhou, H. M. Zhang, C. Cheng, J. M. Ma, W. F. Wei, L. B. Chen and T. H. Wang, *ACS Appl. Mater. Interfaces*, 2013, **15**, 7405-7409.

31 L. Yu, B. Y. Guan, W. Xiao and X. W. Lou, *Adv.Energy Mater.*, 2015, **5**, 1500981.

32 X. H. Lu, G. M. Wang, T. Zhai, M. H. Yu, J. Y. Gan, Y. X. Tong and Y. Li, *Nano Lett.*, 2012, **12**, 1690-1696.

33 T. Zhai, S. L. Xie, M. H. Yu, P. P. Fang, C. L. Liang, X. H. Lu, Y. X. Tong, *Nano energy*, 2014, **8**, 255-263.

Journal of Materials Chemistry A Accepted Manuscript

34 X. Xiao, Z. H. Peng, C.Chen, C. F. Zhang, Majid, B., Z. H. Yang, Y. H. Huang, L. Miao, Yury, G., J. Zhou, *Nano Energy*, 2014, 9, 355-363.

35 X. M, Li, L. F. Jiang, C, Zhou, J. P. Liu and H. B. Zeng, *NPG Asia Materials*, 2015, **7**, e165.

36 T. Zhai, S. L. Xie, M. H. Yu, P. P. Fang, C. L. Liang, X. H. Lu and Y. X. Tong, *Nano Energy*, 2014, **8**, 255-263.

37 J. Graetz, C. C. Ahn, O.Y. Hao, P. Rez, B. Fultz, *Phys. Rev. B*, 2004, **69,** 235103.

38 Z. L. Wang, J. S. Yin, Y. D. Jiang, *Micron,* 2000, **31**, 571-580.

39 S. Stemmer, A. Sane, N. D. Browning and T. J. Mazanec, *Solid State Ionics*, 2000, **130**, 71-80.

40 F. M. F. de Groot, M. Grioni, J. C. Fuggle, J. Ghijsen, G. A. Sawatzky, H. Petersen, *Phys.Rev. B,* 1989, **40**, 5715.

41 P. Gao, Z. C. Kang, W. Y. Fu, W. L. Wang, X. D. Bai and E. G. Wang, *J. Am. Chem. Soc.,* 2010, **132**, 4197-4201.

42 Y. H. Li, Y. F. Zhang, Y. J. Li, Z. Y. Wang, H. Y. Fu. X. N. Zhang, Y. H. Chen, H. Z. Zhang, X. D. Li, *Electrochimica Acta*, 2014, **145**, 177-184.

43 H. Jiang, J. Ma, C. Z. Li, *Chem. Commun.*, 2012, **48**, 4465-4467.

44 D. Z. Kong, W. N. Ren, C. W. Cheng, Y. Wang, Z. X. Huang, H. Y. Yang, *ACS Appl. Mater. Interfaces*, 2015, 7, 21334-21346.

45 H. W. Wang, Z. A. Hu, Y. Q. Chang, Y. L. Chen, H. Y. Wu, Z. Y. Zhang and Y. Y. Yang, *J. Mater. Chem.*, 2011, **21**, 10504-10511.

Journal of Materials Chemistry A Accepted Manuscript

Graphical abstract

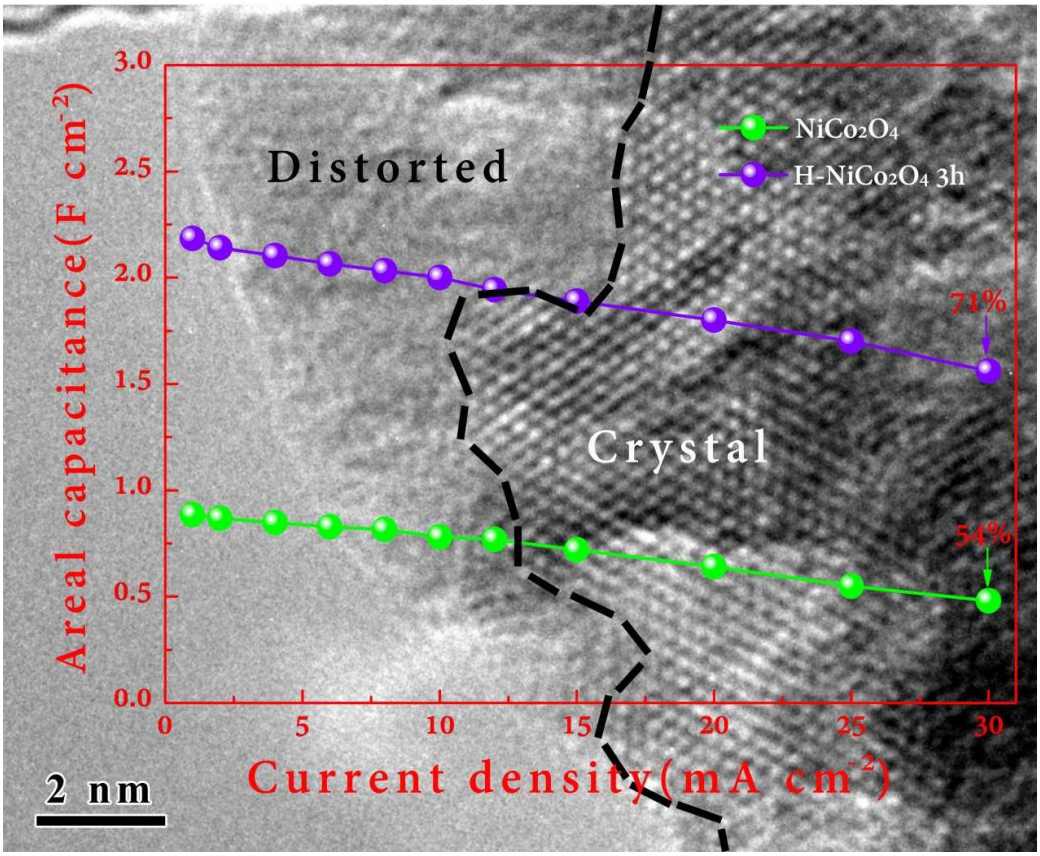

The electrodes of porous $NiCo_2O_4$ nanograss grown *in situ* and supported on Ni foam achieved remarkable enhancement in electrochemical performance through facile hydrogenation. The hydrogenated electrodes exhibited superior comprehensive electrochemical performance compared with the pristine pattern (air-annealed). The prominent electrochemical capacitive properties of hydrogenated $NiCo_2O_4$ are attributed to enhancement in the electrical conductivity observed by *in situ* TEM electrical test, resulting from formation of oxygen vacancies in disordered surface layers (~ 5 nm) observed in the hydrogenated samples.

Journal of Materials Chemistry A Accepted Manuscript